Indian Journal of Engineering & Materials Sciences
Vol. 16, October 2009, pp. 301-309

Fundamental studies on buoyancy-aided conjugate mixed convection with surface radiation from a discretely heated vertical electronic board

S M Sawant & C Gururaja Rao*

Department of Mechanical Engineering, National Institute of Technology, Warangal 506 004, India

Received 15 December 2008; accepted 22 July 2009

The present paper reports numerical results related to the problem of buoyancy-aided conjugate mixed convection with surface radiation from a discretely heated vertical electronic board. The board is equipped with three flush-mounted discrete heat sources of identical dimensions and volumetric heat generation, while air is used as the cooling medium. The governing continuity, Navier-Stokes and energy equations are taken without boundary layer approximations and are solved using finite volume method with the help of stream function–vorticity formulation. An extended computational domain is considered and is discretised with 151 grids along and 111 grids across the board. The nature of variation of local board temperature distribution, peak board temperature, local drag coefficient, mean friction coefficient and relative contributions of mixed convection and radiation to board heat dissipation with reference to some of the pertinent independent parameters has been looked into. Also, some of the contour plots related to isotherm distribution in the computational domain for typical sets of working conditions have been provided.

Keywords: Buoyancy-aided conjugate mixed convection, Surface radiation, Electronic board, Discrete heat sources, Maximum board temperature, Mean friction coefficient

An analytical solution for the problem of fluid flow pertaining to forced convection from an isothermal flat plate was given by Blasius[1]. The geometry of a vertical or horizontal plate has been explored by many researchers[2,3]. Pohlhausen[2] gave analytical solution to forced convection heat transfer from an isothermal flat plate, while Ostrach[3] gave a closed-form solution for laminar free convection from an isothermal vertical flat plate. As far as studies on mixed convection go, Sparrow and Gregg[4] came out with their numerical study on the effect of buoyancy on forced convection fluid flow and heat transfer from a vertical flat plate. Many other researchers[5-7] reported on mixed convection for the plate geometry. The multi-mode heat transfer from the plate geometry was studied by Gorski and Plumb[8], Vynnycky and Kimura[9], Mendez and Trevino[10] and Jahangeer *et al.*[11] In the recent past, studies concerned with mixed convection in conjunction with both conduction and surface radiation are reported by Gururaja Rao[12], who has solved the problem of conjugate mixed convection with radiation from a discretely heated vertical plate containing a single traversable heat source and Kumari and Nath[13] have solved the problem of conjugate mixed convection from a vertical plate moving in a non-Newtonian fluid.

In this paper a numerical study of the problem of buoyancy-aided conjugate mixed convection with surface radiation from a vertical electronic board with three flush-mounted discrete heat sources has been made. Light is thrown on the nature of variation of local drag coefficient, mean friction coefficient, local temperature distribution, peak board temperature, relative contributions of mixed convection and radiation to heat dissipation with reference to a few of the pertinent parameters.

Mathematical Formulation

The schematic diagram of the geometry considered in the present problem is shown in Fig. 1. It consists of a vertical board of height L and thickness t ($<< L$). The board is considered adiabatic on its bottom, left and top surfaces. It consists of three identically dimensioned flush-mounted discrete heat sources of height L_h and thickness t that are placed along the board. The heat generated in the heat sources is conducted along the board and is subsequently dissipated from the right surface of the board by mixed convection and radiation into air, which is taken as the cooling agent. The air flow is induced from the leading edge of the board upwards, and thus one has buoyancy-aided mixed convection coupled with surface radiation.

*For correspondence (E-mail: cgr_gcr@yahoo.co.in)

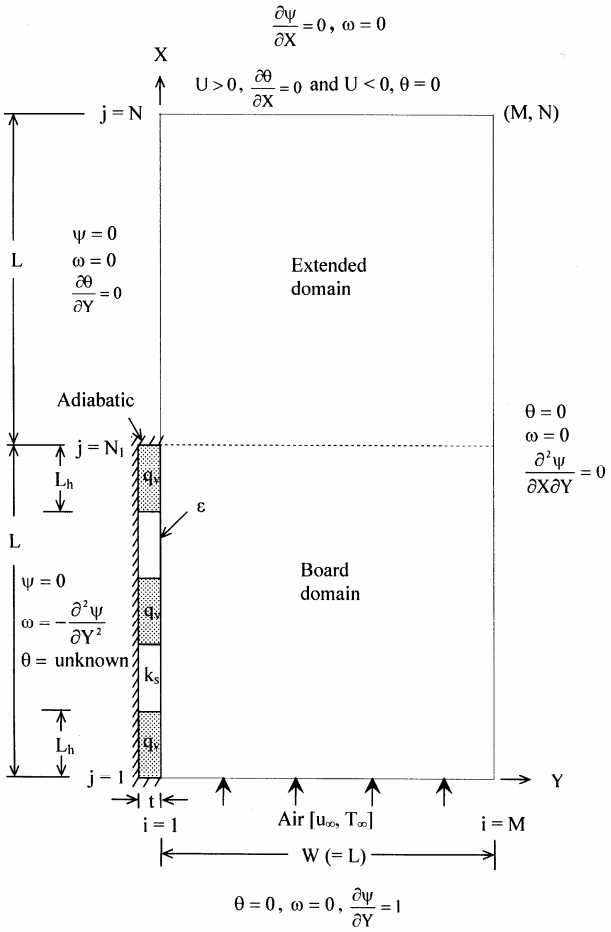

Fig. 1—Schematic of the problem geometry chosen for study along with computational domain and boundary conditions.

The governing equations for the present problem, assuming air to be of constant thermo-physical properties, with Boussinesq approximation considered valid, are the continuity equation, Navier–Stokes equations (*x* and *y* momentum equations) and equation of energy. These equations are transformed into vorticity-stream function form and are later normalised using the appropriate non-dimensional parameters, and these turn out as:

$$U\frac{\partial\omega}{\partial X}+V\frac{\partial\omega}{\partial Y}=-Ri_L^*\frac{\partial\theta}{\partial Y}+\frac{1}{Re_L}\left(\frac{\partial^2\omega}{\partial X^2}+\frac{\partial^2\omega}{\partial Y^2}\right) \quad \ldots (1)$$

$$\frac{\partial^2\psi}{\partial X^2}+\frac{\partial^2\psi}{\partial Y^2}=-\omega \quad \ldots (2)$$

$$U\frac{\partial\theta}{\partial X}+V\frac{\partial\theta}{\partial Y}=\frac{1}{Pe_L}\left(\frac{\partial^2\theta}{\partial X^2}+\frac{\partial^2\theta}{\partial Y^2}\right) \quad \ldots (3)$$

In Eq. (1), Ri_L^* is the modified Richardson number that helps in differentiating the various regimes of mixed convection. The relevant boundary conditions required to solve Eqs (1)-(3) are as shown in Fig. 1. In the present problem, the temperature of the electronic board varies axially on account of the interaction between the heat generated in the three heat sources, the heat conducted along the board, convected and radiated from the board. Owing to this, the governing equations for temperature distribution along the board are obtained by making energy balance. The following elements are to be considered to completely obtain the temperature along the board: (i) elements within the three heat sources, (ii) elements at the interface between heat source and non-heat source portion of the board, (iii) elements in the non-heat source portions of the board and (iv) the bottom and the top adiabatic ends of the board.

As an example, for the element within each of the three discrete heat sources, the energy balance, the accompanying substitution of terms, non-dimensionalization and simplification yields the following equation:

$$\frac{\partial^2\theta}{\partial X^2}+\gamma\left(\frac{\partial\theta}{\partial Y}\right)_{Y=0}+A_{r1}A_{r2}-\varepsilon\gamma N_{RF}\left[\left(\frac{T}{T_\infty}\right)^4-1\right]=0 \quad \ldots (4)$$

Here, the factors A_{r1} and A_{r2} are geometric ratios, and the other parameters γ and N_{RF} are thermal conductance parameter, and radiation-flow interaction parameter, respectively. There are four interface elements separating the heat source and non-heat source portions of the board. As an example, the interface element between the bottommost heat source and the non-heat source portion immediately accompanying it would result in the following normalised version of the governing equation for its temperature:

$$\frac{\partial^2\theta}{\partial X^2}\left[\frac{\Delta X_h}{2}+\frac{\Delta X_{nh}}{2}\right]+\gamma\left(\frac{\partial\theta}{\partial Y}\right)_{Y=0}\left[\frac{\Delta X_h}{2}+\frac{\Delta X_{nh}}{2}\right]+A_{r1}A_{r2}\frac{\Delta X_h}{2}$$
$$-\varepsilon\gamma N_{RF}\left[\left(\frac{T}{T_\infty}\right)^4-1\right]\left[\frac{\Delta X_h}{2}+\frac{\Delta X_{nh}}{2}\right]=0 \quad \ldots (5)$$

By following a similar procedure, the governing equations for the remaining three interface portions of the board may also be obtained. With regard to the two non-heat source portions of the board, for a typical element, the various energy interactions are considered and an energy balance is made in a manner similar to the above cases. This resulted in the

following version of the governing equation for non-dimensional temperature of the non-heat source portions of the board other than interface elements:

$$\frac{\partial^2\theta}{\partial X^2}+\gamma\left(\frac{\partial\theta}{\partial Y}\right)_{Y=0}-\varepsilon\,\gamma\,N_{RF}\left[\left(\frac{T}{T_\infty}\right)^4-1\right]=0 \quad \ldots (6)$$

As far as the bottom and the top adiabatic ends of the board are concerned, a treatment similar to the above is extended and this resulted in the following two equations, respectively, for the bottom and top adiabatic ends:

$$\frac{\partial\theta}{\partial X}+\gamma\frac{\Delta X_h}{2}\left(\frac{\partial\theta}{\partial Y}\right)_{Y=0}+A_{r1}A_{r2}\frac{\Delta X_h}{2}-\varepsilon\,\gamma\,N_{RF}\frac{\Delta X_h}{2}\left[\left(\frac{T}{T_\infty}\right)^4-1\right]=0 \quad \ldots (7)$$

$$\frac{\partial\theta}{\partial X}-\gamma\frac{\Delta X_h}{2}\left(\frac{\partial\theta}{\partial Y}\right)_{Y=0}-A_{r1}A_{r2}\frac{\Delta X_h}{2}+\varepsilon\,\gamma\,N_{RF}\frac{\Delta X_h}{2}\left[\left(\frac{T}{T_\infty}\right)^4-1\right]=0 \quad \ldots (8)$$

Method of Solution and Parametric Range

The normalized governing partial differential equations (1)-(3) are initially transformed into algebraic equations through the finite volume based finite difference method of Gosman *et al*.[14]. Subsequently, the equation set solution is approximated, together with the boundary conditions, using Gauss–Seidel procedure. Stream function and vorticity are relaxed using an under relaxation parameter of 0.5, while on temperature, full relaxation is imposed. The convergence criterion is reached when the residues on stream function, vorticity and temperature become less than 0.0001, 0.0005 and 0.0001, respectively. A computer code has been written for solving the problem.

All calculations are performed taking the height (L) of the board to be 20 cm and thickness (t) to be 1.5 mm, while each discrete heat source is taken to be of height (L_h) 2.5 cm. The free stream temperature of air (T_∞) is 25°C. The thermal conductivity (k_s) of the board is to vary between 0.25 and 1 W/m K. This is done in agreement with earlier published results[15-17], according to which the electronic boards are generally made of materials of thermal conductivity of the order of unity. One example is epoxy glass (coated with Mylar) having thermal conductivity equal to 0.26 W/m K. For surface emissivity (ε) of the board, the lower and upper limits are taken to be 0.05 (a poor emitter) and 0.85 (a good emitter). However, for the specific study meant for exploring the exclusive effect of radiation, ε = 0 and ε = 1 are taken. For modified Richardson number (Ri_L^*), the asymptotic free and forced convection limits are taken to be 25 and 0.1, while $Ri_L^* \approx 1$ signifies pure mixed convection. For volumetric heat generation (q_v), the range is 10^5-10^6 W/m^3. For thermal conductance parameter (γ), which is defined as $[k_f L/k_s t]$, the range is 3.5-14, which, in fact, follows from the range taken for k_s. For radiation-flow interaction parameter (N_{RF}), the suitable range is 22.5-905.5, which also is on account of the ranges fixed for q_v and k_s.

Results and Discussion

Grid independence test

In any numerical study, it is customary to obtain the appropriate grid structure to discretise the computational domain that has been shown in Fig. 1. The three heat source portions of the vertical board are discretised using a finer uniform mesh, while relatively coarser uniform grids are chosen for the two non-heat source portions of the board. In the horizontal direction (across the board), a semi-cosine function is used to generate the mesh. In the extended domain, though in the horizontal direction the same semi-cosine grids, as used in the board region, are continued, in the vertical direction comparatively coarser uniform grids are used.

The grid independence test is made for three typical values of Ri_L^*, namely 0.1, 1 and 25. Of these, in the present paper, the results pertaining to $Ri_L^* = 0.1$ only are provided describing the four stages involved in the study. Table 1 belongs to stage 1 of the study, in which the number of grids in horizontal direction (M) is varied, keeping 20 grids per each heat source and taking $N = 151$ and $N_1 = 101$. It can be seen that, as M changes from 101 to 111, θ_{max} changes by 0.32%, while it changes only by 0.21% as M further increases to 121. Thus, the value of M is fixed at 111 for the entire work. Likewise, Tables 2-4 pertaining to the three subsequent stages of the study indicate the optimum values of N (grids along the vertical direction), N_1 (grids along the board alone) and the number of grids per each heat source to be, respectively, 151, 111 and 24.

Table 1—First stage of grid independence test for Ri_L^*=0.1 (q_v = 10^6 W/m^3, k_s = 0.25 W/m K, ε = 0.45) N = 151, N_1 = 101, number of grids in each heat source = 20

S. No.	M	θ_{max}	Percentage change (abs.)
1	81	0.3357	—
2	91	0.3375	0.54
3	101	0.3387	0.36
4	111	0.3398	0.32
5	121	0.3405	0.21

Table 2—Second stage of grid independence test for Ri_L^*=0.1 (q_v = 10^6 W/m^3, k_s = 0.25 W/m K, ε = 0.45) M = 111, N_1 = 101, Number of grids in each heat source = 20

S. No.	N	θ_{max}	Percentage change (abs.)
1	131	0.3394	—
2	141	0.3396	0.05892
3	151	0.3398	0.05889
4	161	0.3400	0.05886

Table 3—Third stage of grid independence test for Ri_L^*=0.1 (q_v = 10^6 W/m^3, k_s = 0.25 W/m K, ε = 0.45) M = 111, N = 151, number of grids in each heat source = 20

S. No.	N_1	θ_{max}	Percentage change (abs.)
1	91	0.3398	—
2	101	0.3397	0.02943
3	111	0.3396	0.02944
4	121	0.3394	0.05889

Table 4—Fourth stage of grid independence test for Ri_L^*=0.1 (q_v = 10^6 W/m^3, k_s = 0.25 W/m K, ε = 0.45) M = 111, N = 151, N_1 = 111

S. No.	Number of grids in each heat source	θ_{max}	Percentage change (abs.)
1	6	0.3329	-
2	12	0.3375	1.38
3	18	0.3391	0.47
4	24	0.3403	0.35
5	30	0.3410	0.21

Test for energy balance

The results are checked for energy balance for certain typical cases. For this, the total convection and radiation heat dissipation from the board is compared against the net rate of heat generation in the three heat sources in the board. The complete regime of convection ($0.1 \le Ri_L^* \le 25$) is considered, while the other input parameters (k_s, q_v and ε) too have been varied over their corresponding ranges. The energy balance worked out well with the deviations for Ri_L^* = 25, 1 and 0.1 observed to be limited to ± 0.26%, ± 0.09% and ± 0.008%, respectively.

Validation

By asymptotically transforming the present problem to one of mixed convection alone from an isothermal vertical plate, a comparison has been made with the results available in the literature. For the forced convection dominant regime, the works of Blasius[1] and Pohlhausen[2] are considered. For free convection dominant regime, the analytical solution of Ostrach[3] is chosen. With regard to pure mixed convection, the experimental work of Ramachandran *et al*.[6] and the numerical study of Gururaja Rao *et al*.[18] are taken into reckoning. The local velocity distribution, the local temperature distribution and the heat transfer coefficient are taken up for comparison. Good agreement is seen in all the cases. This could be treated as validation for the results of the code generated in the present study.

Study of isotherm plots in different regimes of mixed convection and for different surface emissivities

In order to study the nature of isotherms in the computational domain in different regimes of convection and for different surface emissivities, a family of nine contour plots is obtained as shown in Fig. 2. The entire study made here is for the fixed input comprising q_v = 10^6 W/m^3 and k_s = 0.25 W/m K. The first, second and third rows of the figure correspond to Ri_L^* = 0.1, 1 and 25, respectively. The first, second and third columns [(a), (b) and (c)] correspond to ε = 0.05, 0.45 and 0.85, respectively. The figure clearly shows that, in general, there is a crowding of isotherms at each of the three discrete heat sources present in the board. This expectedly shows major heat transfer activity here. The figure further shows that, for a given surface emissivity, the wall temperature gradient is the steepest for Ri_L^* = 0.1 and gets decreased towards larger values of Ri_L^*. Thus, one can see an increased thermal boundary layer thickness towards larger values of Ri_L^*. The above is expected because, for a fixed surface emissivity, the convection heat transfer would be at its peak for Ri_L^* = 0.1 and at its lowest for Ri_L^* = 25. In contrast to the above, if the isotherm plots are looked at row wise (increasing ε for a given Ri_L^*), one can notice a continuous decrease in crowding of isotherms

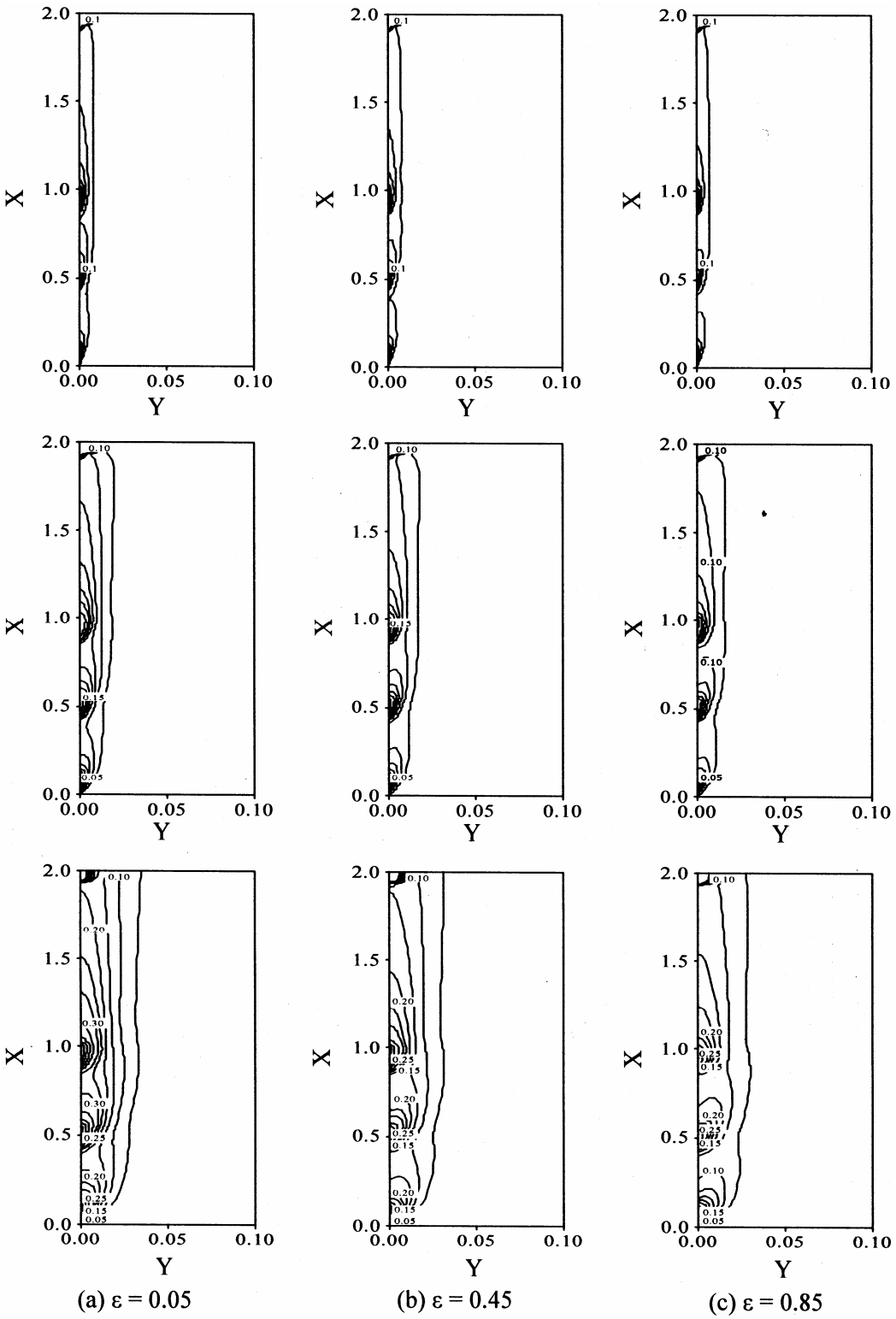

Fig. 2—Isotherm plots in different regimes of mixed convection and for different surface emissivities.

near the heat sources. This implies a progressively decreasing a convection activity with increasing ε in a given convection regime, which should have been compensated by an appropriately increasing radiation activity. In summary, the present study of contour plots throws light on explaining the interplay between convection and radiation in contributing to board heat dissipation.

Study of local non-dimensional temperature distribution along the board

The variation of the non-dimensional local board temperature [θ(*X*)] for different values of thermal conductivity of the board is studied for the case of q_v = 10^6 W/m^3, Ri_L^* = 25 and ε = 0.05. The results are shown in Fig. 3. Four different values of thermal conductivity (k_s) are chosen (0.25, 0.5, 0.75 and 1 W/m K). It is to be kept in mind that θ(*X*) is defined equal to $\left[\left(T(x)-T_\infty\right)\right]/\Delta T_{ref}$, where $\Delta T_{ref} = \left(q_v L_h t/k_s\right)$. In view of this, as k_s increases, ΔT_{ref} decreases and thus θ(*X*) increases, though in reality there would be a drop in *T*(*x*) with increasing k_s. For a given value of k_s, the local non-dimensional board temperature profile shows three peaks, with the last peak occurring near the trailing edge of the board being the maximum. Since increasing value of k_s means enhanced internal conduction through the board there is an expected drop in the local board temperature. In the present example, as k_s increases from 0.25 to 1 W/m K, θ(*X*) increases by 288.90%, which translates to a decrease in *T*(*x*) by 2.32% near the trailing edge of the board. The smaller drop in *T*(*x*) could be attributed to the smaller values of k_s (in the range between 0.25 to 1 W/m K) chosen for study. The selection of the above range for k_s is again due to the reasons already spelt out under ranges of parameters.

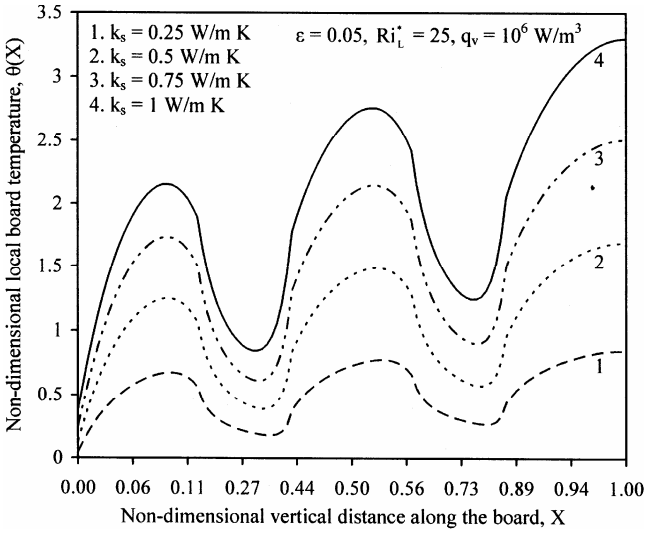

Fig. 3—Variation of non-dimensional local board temperature with thermal conductivity of the board.

Exclusive effect of surface radiation on maximum non-dimensional board temperature

In an attempt to isolate the role of surface radiation in the present study, Fig. 4 has been plotted. It shows the variation of maximum non-dimensional board temperature in different regimes of convection ($0.1 \le Ri_L^* \le 25$) without and with the effect of radiation taken into reckoning. The study is made for ε = 0 (radiation absent) and ε = 1 (best possible radiation). It may be noted that radiation has a significant role in checking the maximum board temperature in all the regimes of convection. In particular, the dominance of radiation reaches its peak towards larger values of Ri_L^* (free convection dominant regime). In the sample case pertaining to Fig. 4, a comparison with the situation that omits radiation shows that consideration of radiation (with ε = 1) brings down θ_{max} by 22.92%, 34.32% and 40.97% for Ri_L^* = 0.1, 1 and 25 respectively. The above highlights the role radiation assumes in this problem.

Relative contributions of mixed convection and surface radiation

The dissipation of heat from the board is shared by mixed convection and radiation. In view of this, a

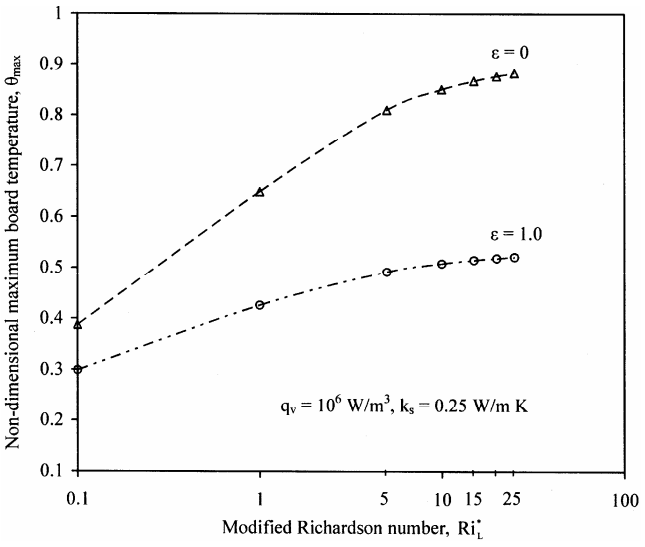

Fig. 4—Non-dimensional peak board temperature in various regimes of convection highlighting the exclusive role of surface radiation.

study is made to delineate the contributions from mixed convection and radiation in various regimes of convection. Figure 5 shows this for the case with q_v= 10^6 W/m^3 and k_s = 0.25 W/m K. Five typical values of surface emissivity are chosen, namely ε = 0.05, 0.25, 0.45, 0.65 and 0.85, and three different regimes of convection (Ri_L^* = 25, 1 and 0.1) are selected. The figure indicates that, in a given regime of convection, the contribution to heat dissipation by convection progressively decreases as ε rises from 0.05 to 0.85, with the contribution from radiation showing a mirror image increase. However, for Ri_L^* = 0.1, indicating forced convection dominance, there is an expected lead role taken by convection, with radiation showing a limited effect. In the present example, for Ri_L^* = 0.1, the contribution from convection is ranging between 98.40% and 78.88% as ε changes from 0.05 to 0.85. In contrast, here, radiation is contributing a maximum of only 21.12% for the upper limit of emissivity (0.85) chosen. As one moves towards pure mixed convection (Ri_L^* = 1), radiation starts playing an enhanced role, with its contribution to heat dissipation increasing from 3.03% to 32.94% as ε varies from 0.05 to 0.85. In the regime of free convection dominance (Ri_L^* = 25), radiation is at its best, with as much as 45.94% contributed by it for the value of ε = 0.85.

Variation of local drag coefficient with other parameters

The pumping power required to cause the fluid (air) flow past the board depends on the induced (free-stream) velocity, u_∞, and the drag coefficient. Hence, the nature of variation of the local drag coefficient (C_{f_x}) with reference to pertinent governing parameters is probed here. Figure 6 depicts local drag coefficient profiles for different surface emissivities. For a given surface emissivity, as one moves from the leading edge of the board, the local drag coefficient decreases sharply to a minimum. From here, C_{f_x} increases again and is reaching a local peak near the top end of the bottom most heat source, from where it decreases once again. After reaching a local minimum, C_{f_x} shoots up one more time along the central heat source. Beyond the central heat source, C_{f_x} again decreases, and after attaining another local minimum, it rises and reaches its maximum at the top adiabatic end of the board. In summary, each of the three curves shown in Fig. 6 contains three local maxima and three local minima. The first local minimum is the least of the three minima, while the last local peak turns out to be the maximum local drag coefficient that the fluid encounters. The figure also explains that increasing surface emissivity brings down C_{f_x} at a given location along the board in any given regime of convection. In the present example, the maximum local drag coefficient is decreasing by 18.26% as ε increases from 0.05 to 0.45, while for a further rise in ε to 0.85, C_{f_x} drops down by another 13.31%.

Relative contributions of forced and free convection components in mean friction coefficient

The mean friction coefficient ($\bar{C}_f$) experienced by the fluid is contributed both by free and forced

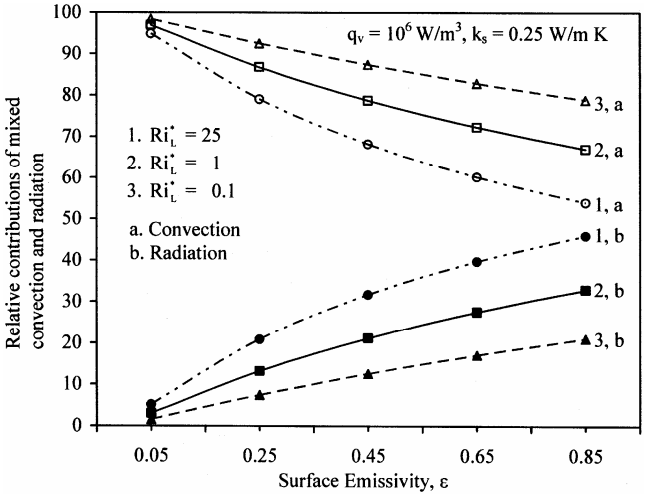

Fig. 5—Relative contributions of mixed convection and radiation with surface emissivity in different regimes of mixed convection.

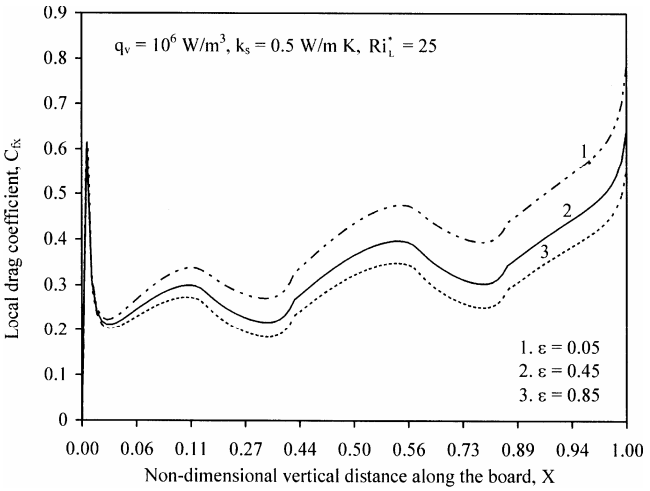

Fig. 6—Variation of local drag coefficient along the board for different surface emissivities.

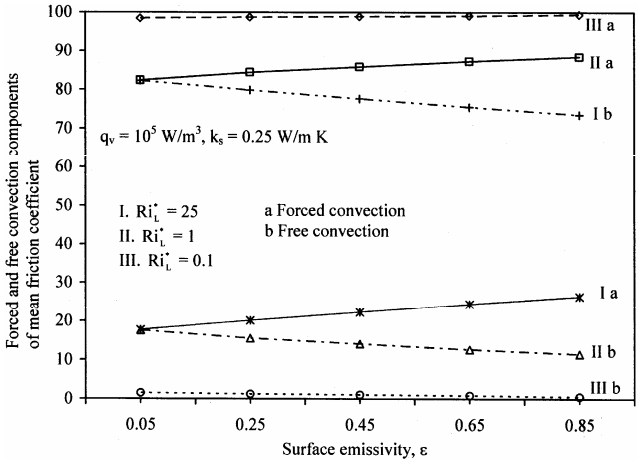

Fig. 7—Forced and free convection components of mean friction coefficient plotted against surface emissivity in different regimes of convection.

convection components in the present mixed convection problem. It has been decided to look at the relative roles that free and forced convection play in influencing $\overline{C}_f$ in various regimes of convection (Fig. 7). This figure shows that, for $Ri_L^* = 25$, the contribution from free convection to $\overline{C}_f$ is expectedly far greater than that from forced convection. Also, for the same Ri_L^*, the figure reveals an almost linear decrement in the contribution from free convection to $\overline{C}_f$ with increasing ε, while there is a mirror-image increment in the contribution provided by forced convection. In contrast, for $Ri_L^* = 1$ (pure mixed convection) and $Ri_L^* = 0.1$ (asymptotic forced convection), the dominance of forced convection over free convection may be seen in influencing the value of $\overline{C}_f$. Further, in these two cases, the contribution from forced convection almost linearly increases with increasing ε, with the corresponding free convection counterparts showing a mirror-image variation. In the present example, for $Ri_L^* = 25$, when one uses a board with ε = 0.45, free convection contributes 77.67% to $\overline{C}_f$, with the remaining 22.33% provided by forced convection. In contrast, for the same ε = 0.45, when working in forced convection limit ($Ri_L^* = 0.1$), forced convection overpowers free convection contributing 98.92% to $\overline{C}_f$. The above study clearly states that the role of free convection in pumping power cannot be overlooked, specifically while operating in the regime of $Ri_L^* \geq 1$. As far as forced convection contribution goes, it cannot be ignored no matter what the regime of operation is in view of the fact that its contribution ranges from a low of 17.73% to a high of 99.42%.

Conclusions

The problem of multi–mode heat transfer from a discretely heated, conducting, vertical board has been studied. A computer code for the purpose has been written. An extended computational domain both along and across the board is chosen and an optimum grid system is used for discretizing the computational domain. The effects of different governing parameters, viz., modified Richardson number, emissivity and thermal conductivity, on fluid flow results (local drag coefficient and mean friction coefficient) and heat transfer results (local board temperature, peak board temperature and contributions of different modes of heat transfer to heat dissipation) are studied. The exclusive role of radiation in deciding the results of the present problem is elucidated.

Nomenclature

A_{r1}, A_{r2}	=	geometric ratios, L/t and L/L_h, respectively
$\overline{C}_f$	=	mean friction coefficient
C_{f_x}	=	local drag coefficient along the board
Gr_L^*	=	modified Grashof number, $g \beta \Delta T_{ref} L^3 / \nu_f^2$
k_f	=	thermal conductivity of air, W/m K
k_s	=	thermal conductivity of the board material and heat source, W/m K
L, L_h, t	=	heights of board and heat source and thickness of both, respectively, m
M, N	=	number of grids in Y and X directions, respectively
N_1	=	number of grids on the board
N_{RF}	=	radiation-flow interaction parameter, $\sigma T_\infty^4 / \left[\left(k_f \Delta T_{ref} \right) / L \right]$
Pe_L	=	Peclet number, $Re_L Pr$ or $u_\infty L/\alpha$
Pr	=	Prandtl number of air
q_v	=	rate of volumetric heat generation in each discrete heat source, W/m^3
Re_L	=	Reynolds number, $u_\infty L/\nu_f$
Ri_L^*	=	modified Richardson number, $(g \beta \Delta T_{ref} L)/u_\infty^2$ or $[Gr_L^* / Re_L^2]$
T, T_{max}	=	local and maximum temperatures in the computational domain, respectively, K or °C
T_∞	=	free stream temperature of air, K or °C
u, v	=	vertical and horizontal components of velocity, respectively, m/s
u_∞	=	free stream velocity of air, m/s
U, V	=	non–dimensional vertical and horizontal velocities, respectively, u/u_∞ and v/u_∞
W	=	width of the computational domain, m
x, y	=	vertical and horizontal distances, respectively, m

X, Y = non–dimensional vertical and horizontal distances, x/L, y/L, respectively

Greek symbols

γ = thermal conductance parameter, $[k_f L/k_s t]$

β = isobaric cubic expansivity of air, $-(1/\rho)\times(\partial\rho/\partial T)_P$, K^{-1}

ΔT_{ref} = modified reference temperature difference, K or °C, $q_v L_h t/k_s$

ΔX_h = non-dimensional height of the board element chosen for energy balance in heat source portion

ΔX_{nh} = non-dimensional height of the board element chosen for energy balance in non-heat source portion

E = surface emissivity of the board

Θ = non–dimensional local temperature, $(T-T_\infty)/\Delta T_{ref}$

θ_{max} = non–dimensional peak board temperature

ν_f = kinematic viscosity, m^2/s

ρ, ρ_∞ = local and characteristic values of fluid density, respectively, kg/m^3

σ = Stefan–Boltzmann constant (= 5.6697×10^{-8} $W/m^2 K^4$)

ψ = non–dimensional stream function, $\psi'/u_\infty L$

ψ' = stream function, m^2/s

ω = non–dimensional vorticity, $\omega' L/u_\infty$

ω' = vorticity, s^{-1}

References

1 Blasius H, *Z. Math Phys*, 56 (1908) 1.

2 Pohlhausen H, *ZAMM*, 1 (1921) 115.

3 Ostrach S, *NACA Rep,* 1111 (1953).

4 Sparrow E M & Gregg J L, *ASME J Appl Mech*, 81 (1959) 133.

5 Lloyd J R & Sparrow E M, *Int J Heat Mass Transfer*, 13 (1970) 434.

6 Ramachandran N, Armaly B F & Chen T S, *ASME J Heat Transfer*, 107 (1985) 636.

7 Chen T S, Armaly B F & Ramachandran N, *ASME J Heat Transfer*, 108 (1986) 835.

8 Gorski M A & Plumb O A, *Proc Winter Ann Meet ASME, ASME HTD*-210, (1992) 99-105

9 Vynnycky M & Kimura S, *Int J Heat Mass Transfer*, 39, (1996) 1067.

10 Mendez F & Trevino C, *Int J Heat Mass Transfer*, 43, (2000) 2739.

11 Jahangeer S, Ramis M K & Jilani G, *Int J Heat Mass Transfer*, 50 (2007) 85.

12 Gururaja Rao C, *Numer Heat Transfer A*, 45 (2004) 935.

13 Kumari M & Nath G, *Int J Thermal Sci*, 45 (2006) 607.

14 Gosman A D, Pun W M, Runchal A K, Spalding D B & Wolfshtein M, *Heat and Mass Transfer in Recirculating Flows* (Academic Press, New York), 1969.

15 Peterson G P & Ortega A, in *Advances in Heat Transfer*, edited by Hartnett J P and Irvine Jr. T F (Academic Press, San Diego, California), 1990, 181.

16 Gururaja Rao C, Venkata Krishna A & Naga Srinivas P, *Numer Heat Transfer A*, 48 (2005) 427.

17 Gururaja Rao C, *Numer Heat Transfer A*, 52 (2007) 1.

18 Gururaja Rao C, Balaji C & Venkateshan S P, *Int J Transport Phenomena*, 2 (2000) 143.